Research in Astronomy and Astrophysics, 25:015013 (15pp), 2025 January

https://doi.org/10.1088/1674-4527/ada05f
CSTR: 32081.14.RAA.ada05f

Study on the One-year Accuracy of Pulsar Time-scale

Linlin Wang[1,2,3], Zhehao Zhang[1,2,3], Chengshi Zhao[1,2], Zongke Li[1,2,3], and Minglei Tong[1,2,3]
[1] National Time Service Center, Chinese Academy of Sciences, Xi'an 710600, China; mltong@ntsc.ac.cn
[2] Key Laboratory of Time Reference and Applications, Chinese Academy of Sciences, Xi'an 710600, China
[3] University of Chinese Academy of Sciences, Beijing 100049, China
Received 2024 November 30; revised 2024 December 11; accepted 2024 December 14; published 2025 January 8

Abstract

Determining accurate pulsar timing model parameters is essential for establishing TT(PT), a realization of Terrestrial Time (TT) based on a pulsar timescale (PT). This study discusses the impact of different data spans on the accuracy of pulsar timing model parameters when determining pulsar timing model parameters. Using observations of PSR J0437-4715, J1909-3744, J1713+0747, and J1744-1134 from the second data release of the International Pulsar Timing Array (IPTA II, Version A), we compare the accuracy of the timing model parameters determined by these observations with different data spans. The results show for PSR J0437-4715, J1713+0747, and J1909-3744, the amplitude fluctuations of rotational frequency remain within 10^{-15}, 10^{-14}, and 10^{-14} Hz, respectively, when the data spans for determining pulsar timing model parameters exceed 13, 14, and 6 yr. Additionally, the one-year accuracy of TT(PT) is crucial for its application in timekeeping. By comparing the frequency deviations of TT(PT) relative to TT(BIPM) under both ideal (k_r) and actual (k_p) conditions across different data spans, we find that when the data span reaches the duration above, the accuracy of TT(PT) surpasses that of TT(TAI) under ideal conditions, slightly inferior under actual conditions. This suggests with improved observational technologies, the accuracy of TT(PT) can be further enhanced.

Key words: (stars:) pulsars: individual (PSRs J1909-3744, J1713+0747, J0437-4715, J1744-1134) – time – methods: data analysis

1. Introduction

Pulsars are neutron stars with rapid rotation and high magnetism, formed in the gravitational collapse of some massive stars (Lyne & Graham-Smith 2012). Since the first discovery of pulsar, PSR B1919+21, pulsar science has gradually developed (Hewish et al. 1968). Before long, Reichley et al. (1971) proposed that the pulsar signal could be used as a clock signal. Especially, after the first millisecond pulsar, PSR B1937+21, was discovered, the development of pulsar timing applications were significantly advanced (Backer et al. 1982). Millisecond pulsars are honored as nature's most stable clocks for their extraordinary rotational stability (Taylor 1991). Some millisecond pulsars have fractional stabilities comparable to those of the best atomic clocks at that time (Taylor 1991). Since then, millisecond pulsar timing has attracted much attention from astronomers. In recent years, with the discovery of more millisecond pulsars and the development of the observational equipment and technology, millisecond pulsar timing applications in pulsar timescale has been studied by many researchers (Rodin 2008; Hobbs et al. 2012, 2020; Zhang et al. 2024). Pulsar timing applications depend on the stability of pulsar rotation, with precise measurements of their rotational parameters being fundamental to related research. However, due to the vast distances of pulsars from Earth, an accurate pulsar timing model is essential for steering the pulsar timescale (PT) to the reference timescale that conforms to the International System of Units (SI), thereby obtaining a realization of Terrestrial Time (TT) based on PT, denoted as TT(PT) (Hobbs et al. 2012; Tong et al. 2017). Hobbs et al. (2006) developed a pulsar timing package, Tempo2, based on pulsar timing principles. Employing Tempo2 to analyze the long-term pulsar timing observations, the pulsar timing model parameters are precisely determined (Edwards et al. 2006). With the increasing number of pulsar timing observations, the precision of the pulsar timing model parameters is correspondingly enhanced (Tong et al. 2017).

The pulsar timing observation is the process of measuring pulsar timing model parameters using TT(BIPM) as the time reference, which is equivalent to establishing the pulsar timescale with TT(BIPM) as the reference. TT(BIPM) is a realization of Terrestrial Time (TT) as defined by the International Astronomical Union (IAU), which is released once a year. Consequently, on a one-year timescale, the accuracy of TT(PT) that is predicted by these model parameters is crucial for evaluating its feasibility as a time reference. Accordingly, this paper focuses on the accuracy of TT(PT) on a one-year timescale. To clearly distinguish between different yearly versions of TT(BIPM), an alternative notation, TT(BIPMXX), is used. TT(BIPMXX) is computed and

updated by the Bureau International des Poids et Mesures (BIPM), based on a weighted average of the evaluations of the frequency of the International Atomic Time (TAI) by the primary and secondary frequency standards, and XX corresponds to the year of the most recent data used (Guinot & Petit 1991). For example, TT(BIPM15) represents the version released in 2015 (Petit 2004). TAI is obtained by the BIPM using the ALGOS algorithm to comprehensively process the data generated by more than 450 high-accuracy atomic clocks worldwide in the past month, which is released once a month (Panfilo & Arias 2009). TT(TAI) is another realization of TT, which defined as TT(TAI) = TAI+32.184 s. When TT(BIPM) has not been released, TT(TAI) is typically used as the time reference. Long-term and high-precision pulsar timing observations are fundamental to determining accurate pulsar timing model parameters. At present, the pulsar timing arrays that have been built in the world mainly include the European Pulsar Timing Array (EPTA; Desvignes et al. 2016), the North American Pulsar Timing Array (NANOGrav; Arzoumanian et al. 2020), the Parkes Pulsar Timing Array (PPTA; Reardon et al. 2021), the Indian Pulsar Timing Array (InPTA; Tarafdar et al. 2022), MeerKAT Pulsar Timing Array (MPTA; Johnston et al. 2020), Chinese Pulsar Timing Array (CPTA; Lee 2016) and so on. The International Pulsar Timing Array (IPTA), a combination of the EPTA, NANOGrav, and PPTA, released the second pulsar timing observations (IPTA DR2) in 2019, containing a total of 65 millisecond pulsars (Perera et al. 2019). These timing observations are the most essential foundation for pulsar timing research and gravitational wave detection.

The parameters of different pulsar timing models can be determined by using pulsar timing observations with different spans. The most accurate pulsar timing model parameters can only be determined by choosing the appropriate data span. In this paper, based on IPTA DR2, we select a few millisecond pulsars with excellent performance to determine different pulsar timing model parameters with different observation spans for exploring the optimal data span. Since IPTA DR2 uses TT(BIPM15) as the time reference, this paper also adopts TT(BIPM15) as the time reference. Additionally, on the one-year timescale, the accuracy of the different model parameters and the TT(PT) of these parameter forecasts are studied.

2. Pulsar Timing Model

The accurate pulsar timing model parameters are fundamental to the application of pulsar timekeeping. These parameters mainly include the rotation frequency (ν) of the pulsar, the first derivative ($\dot{\nu}$) of the rotation frequency, the second derivative ($\ddot{\nu}$) of the rotation frequency, the R.A., the decl., the parallax, the proper motion, the binary orbital parameters, and so on. We can determine the pulsar timing model parameters based on the arrival time of pulse (TOA), combined with the least-squares method. This is also the process of constructing a pulsar clock. During the observation of TOA, we use the local station atomic clock to record the TOA, denoted as $t_{\rm obs}$. To ensure the accuracy of the pulsar timing data, one needs to trace $t_{\rm obs}$ to TT(BIPM) during various time corrections. The arrival of pulsar signals at ground-based telescopes involves various physical processes and geometric effects, and an accurate pulsar timing model is needed to relate TOA at the Solar System Barycenter (SSB), $t_{\rm ssb}$, to $t_{\rm obs}$, which can be expressed as (Edwards et al. 2006):

$$t_{\rm SSB} = t_{\rm obs} - (\Delta_{\rm A} + \Delta_{\rm R\odot} + \Delta_{\rm p} + \Delta_{\rm D\odot} + \Delta_{\rm E\odot} + \Delta_{\rm S\odot}) \quad (1)$$

where $\Delta_{\rm A}$ denotes the atmospheric delays; $\Delta_{\rm R\odot}$ denotes the Roemer delay, which is the simple vacuum delay between the arrival of the pulse at the observatory and the SSB; $\Delta_{\rm p}$ denotes the delays caused by the parallax; $\Delta_{\rm D\odot}$ denotes the dispersion delays caused by the interstellar medium; $\Delta_{\rm E\odot}$ denotes the Einstein delay related to the relativistic four-dimensional spacetime transformation; and $\Delta_{\rm S\odot}$ denotes the Shapiro delay, which is an excess time delay caused by the passage of the pulse through curved spacetime. These delay terms can be expressed in detail as (Edwards et al. 2006; Tong et al. 2017):

$$\begin{aligned}\Delta_{\rm R\odot} = &-\frac{1}{c}(\hat{\boldsymbol{n}}\cdot\boldsymbol{r}) - \frac{1}{cR_0}[\boldsymbol{v}\cdot\boldsymbol{r} - (\hat{\boldsymbol{n}}\cdot\boldsymbol{v})(\hat{\boldsymbol{n}}\cdot\boldsymbol{r})]\,\Delta t \\ &+ \frac{1}{2cR_0^2}(\hat{\boldsymbol{n}}\cdot\boldsymbol{r})[v^2 - (\hat{\boldsymbol{n}}\cdot\boldsymbol{v})^2]\,\Delta t^2 \\ &+ \frac{1}{cR_0^2}(\hat{\boldsymbol{n}}\cdot\boldsymbol{v})[\boldsymbol{v}\cdot\boldsymbol{r} - (\hat{\boldsymbol{n}}\cdot\boldsymbol{v})(\hat{\boldsymbol{n}}\cdot\boldsymbol{r})]\,\Delta t^2 \end{aligned} \quad (2)$$

$$\begin{aligned}\Delta_{\rm E\odot} = &\frac{1}{c^2}\int_{t_0}^{t}\left[U_\oplus + \frac{v_\oplus^2}{2} + \Delta L_{\rm C}^{\rm (PN)} + \Delta L_{\rm C}^{\rm (A)}\right]dt \\ &+ \frac{\boldsymbol{s}\cdot\dot{\boldsymbol{r}}_\oplus + W_0 t_{\rm obs}}{c^2}\end{aligned} \quad (3)$$

$$\Delta_{S\odot} = -\sum_{k=1}^{l}\frac{2GM_k}{c^3}\ln|\hat{\boldsymbol{n}}\cdot\boldsymbol{r_k} + r_k| + \frac{4G^2M_\odot^2}{c^5 r_\odot\tan\psi\sin\psi} \quad (4)$$

$$\Delta_{\rm p} = \frac{1}{2cR_0}[r^2 - (\hat{\boldsymbol{n}}\cdot\boldsymbol{r})^2] \quad (5)$$

$$\Delta_{\rm D\odot} = \frac{\rm DM_\odot}{2.410\times10^{-16}\,{\rm cm^{-3}\,pc}}(f^{\rm SSB})^{-2} \quad (6)$$

where c denotes the speed of light. $\hat{\boldsymbol{n}}$ is the unit vector of the pulsar in the Barycentric Celestial Reference System (BCRS). $\boldsymbol{r}$ is the position vector of the telescope at the moment of observation. $\boldsymbol{v}$ is the pulsar velocity vector relative to the SSB. $\Delta t = t - t_0$, where t_0 is a reference epoch. R_0 denotes the distance of the pulsar to the SSB at t_0. $U_\oplus$ is the gravitational potential at the geocenter caused by all solar system bodies except the Earth. $v_\oplus$ is the velocity of the geocenter relative to the SSB. $\Delta L_{\rm C}^{\rm (PN)}$ and $\Delta L_{\rm C}^{\rm (A)}$ apply a correction for higher-order relativistic terms, with $\Delta L_{\rm C}^{\rm (PN)} = 1.097\times10^{-16}$ and $\Delta L_{\rm C}^{\rm (A)} = 5\times10^{-18}$. $\boldsymbol{s}$ is a vector from the geocenter to the observatory. $\dot{\boldsymbol{r}}_\oplus$ is the velocity of the geocenter with respect to the barycenter. $W_0 = 6.969290134\times10^{-10}c^2$ approximates the

Table 1
Information of Parameters of the Four Millisecond Pulsars

Pulsar Name	Time Span (yr)	ν (Hz)	$\dot{\nu}$ (s^{-2})	Residual rms (μs)	Number of TOAs
J0437-4715	18.6	173.6879457375184085	−1.72837479203367628 71E-15	0.245	5302
J1713+0747	22.5	218.81184041715810527	−4.083853596017421807E-16	0.242	17457
J1909-3744	10.8	339.31568721848368025	−1.614822573518876169E-15	0.190	11483
J1744-1134	19.9	245.42611968980827857	−5.381659879050442 3769E-16	0.832	9834

gravitational plus spin potential of the Earth at the geoid. G is Newton's gravitational constant. M_k denotes the mass of the kth solar system object. $\boldsymbol{r_k}$ denotes the position vector of the telescope relative to the kth solar system object at the moment of observation. r_k is modulo $\boldsymbol{r_k}$, and l denotes the number of major solar system objects used in the calculation of the Shapiro delay. $r_\odot$ denotes the distance from the telescope to the Sun at the moment of observation. $M_\odot$ denotes the solar mass, and ψ denotes the tensor angle of the Sun and the pulsar to the telescope at the moment of observation. f^{SSB} is the observing frequency transformed to the barycentric frame. $\mathrm{DM}_\odot$ is a dispersion measure due to the interplanetary medium.

After converting t_{obs} to t_{ssb}, we can get the observed rotation phase $\phi(t_{\mathrm{ssb}})$ and the theoretical forecast rotation phase $N(t_{\mathrm{ssb}})$ based on the pulsar phase model, which can be expressed as (Petit et al. 2019):

$$\phi(t_{\mathrm{ssb}}) = \phi_0 + \nu(t_{\mathrm{ssb}} - t_0) + \frac{1}{2}\dot{\nu}(t_{\mathrm{ssb}} - t_0)^2 + \frac{1}{6}\ddot{\nu}(t_{\mathrm{ssb}} - t_0)^3 + \cdots \quad (7)$$

where ϕ_0 is the phase at t_0, ν is the rotation frequency, and $\dot{\nu}$ and $\ddot{\nu}$ are the first and second derivatives of the rotation frequency, respectively. $N(t_{\mathrm{ssb}})$ is always the nearest integer to $\phi(t_{\mathrm{ssb}})$. The differences between the two kinds of rotation phases are the so-called timing residuals, which can be expressed as (Davis et al. 1985):

$$R_i = \frac{\phi_i - N_i}{\nu} \quad (8)$$

where ϕ_i is the measured ith pulse phase, R_i is the ith timing residuals. Based on the actual process of pulsar timing observations, we trace t_{obs} to TT(BIPM15) during various time corrections in this paper. Without any fitting operation, R_i is called the pre-fit timing residuals. To obtain accurate pulsar timing model parameters, we perform a least squares fit to the pre-fit timing residuals using the following formula:

$$\chi^2 = \sum_{i=1}^{N}\left(\frac{R_i}{\sigma_i}\right)^2 \quad (9)$$

where σ_i represents the uncertainty in R_i. We minimize χ^2 using the least squares method to obtain new model parameters. This fitting process is repeated until the residuals level off within the computational precision. Eventually, accurate timing model parameters and post-fit timing residuals are obtained. Theoretically, once pulsar timing model parameters are determined, they remain valid over a long period. However, model parameters obtained by using different data spans are different. To obtain the optimal data span for determining pulsar timing model parameters, we discuss the impact of different data spans on model parameters.

3. Accuracy Analysis of Pulsar Timing Model Parameters

To obtain the accurate pulsar timing model parameters, we can determine these timing model parameters with different data spans and analyze the accuracy of these parameters. When the differences between these pulsar timing model parameters are minimal, these parameters tend to level off. To avoid complexity, this paper only analyzes the accuracy of rotation parameters (ν, $\dot{\nu}$) determined with different data spans and the accuracy of the pre-fit timing residuals predicted by these parameters.

3.1. Methods for Determining Pulsar Timing Model Parameters

To determine accurate pulsar timing model parameters, selecting appropriate pulsar timing observations is also crucial. Based on the observations released by IPTA DR2, we select PSR J1909-3744, J0437-4715, J1713+0747, and J1744-1134, which have high timing precision (Verbiest et al. 2016; Perera et al. 2019) compared to others. Their information is shown in Table 1, and their post-fit timing residuals are shown in Figure 1. In the process of determining the pulsar timing model parameters, the parameters that need to be fitted include the rotation frequency, the first derivative of the rotation frequency, R.A., decl., proper motion, parallax, dispersion, and so on. Additionally, since PSR J1909-3744, J0437-4715, and J1713 +0747 are binary systems, binary parameters also need to be fitted, including the orbital period, the derivative of the orbital period, the projected semimajor axis of the orbit, the longitude of periastron, the rate of advance of periastron, the orbital eccentricity, the companion mass, and others. We first

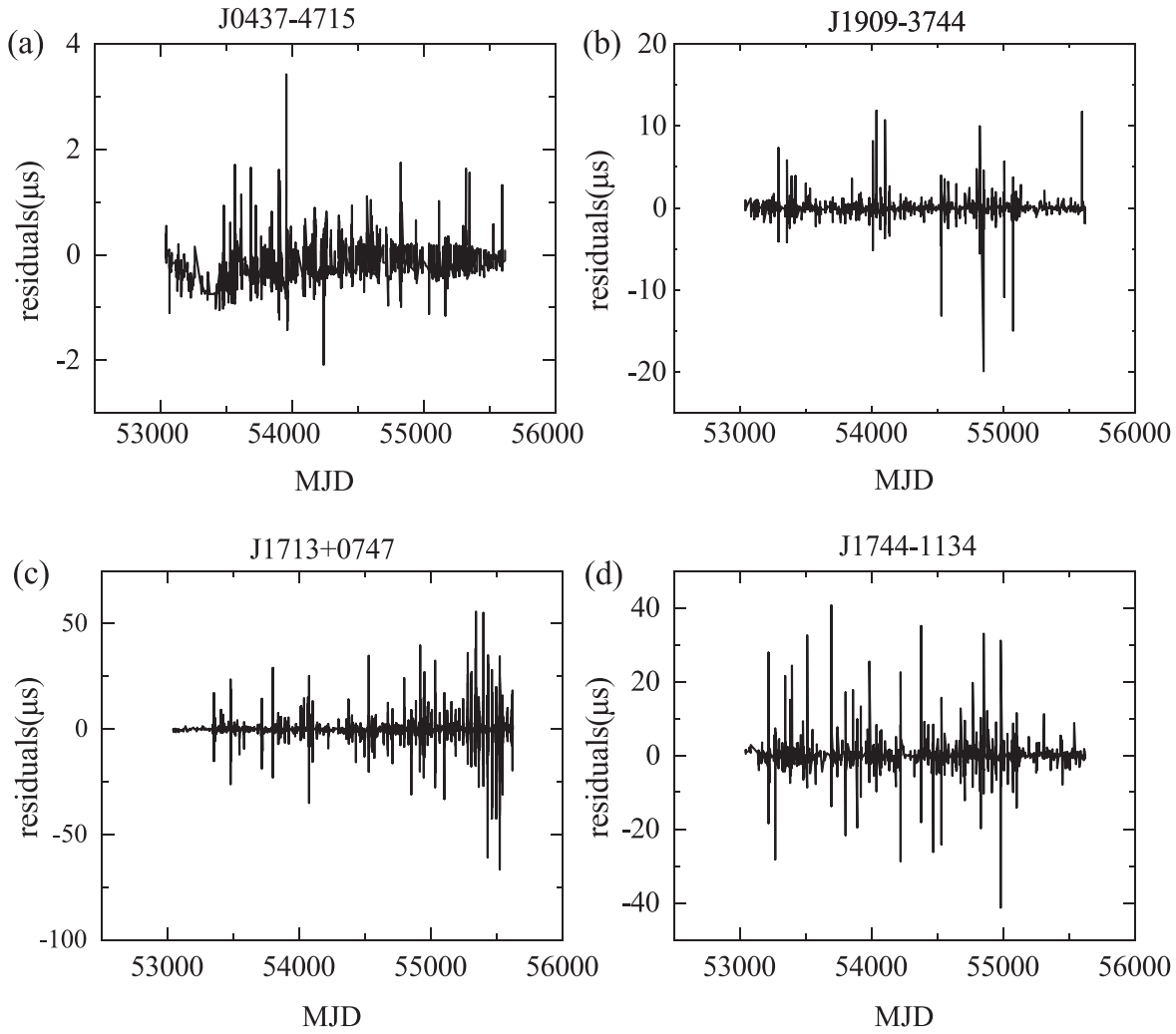

Figure 1. Post-fit timing residuals of four millisecond pulsars. (a) Post-fit timing residuals of PSR J0437-4715 at MJD from 50191 to 56978. (b) Post-fit timing residuals of PSR J1909-3744 at MJD from 53040 to 56993. (c) Post-fit timing residuals of PSR J1713+0747 at MJD from 48849 to 57053. (d) Post-fit timing residuals of PSR J1744-1134 at MJD from 49728 to 56992.

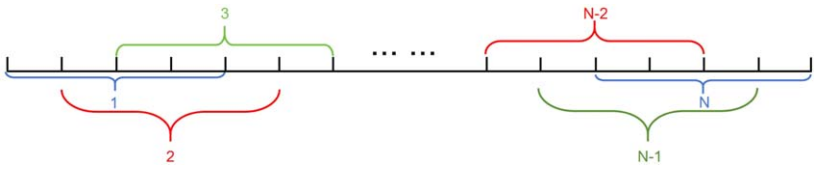

Figure 2. Schematic diagram of the data spans for determining pulsar timing model parameters division.

determine the model parameters using four-year observations through the following steps:

(1) First, using the reference epoch(PEPOCH) 55000 provided by IPTA DR2, we employ Tempo2 to fit the pulsar timing model parameters with four-year observational data until convergence. Then we output these parameters such as ν, $\dot{\nu}$, and obtain the corresponding uncertainties, denoted as $\nu_{\rm err}$ and $\dot{\nu}_{\rm err}$.

(2) Second, we fix the four-year data span but move with a step of one year, as shown in Figures 2. Repeat step (1). For example, with J0437-4715, which has an 18.6 yr

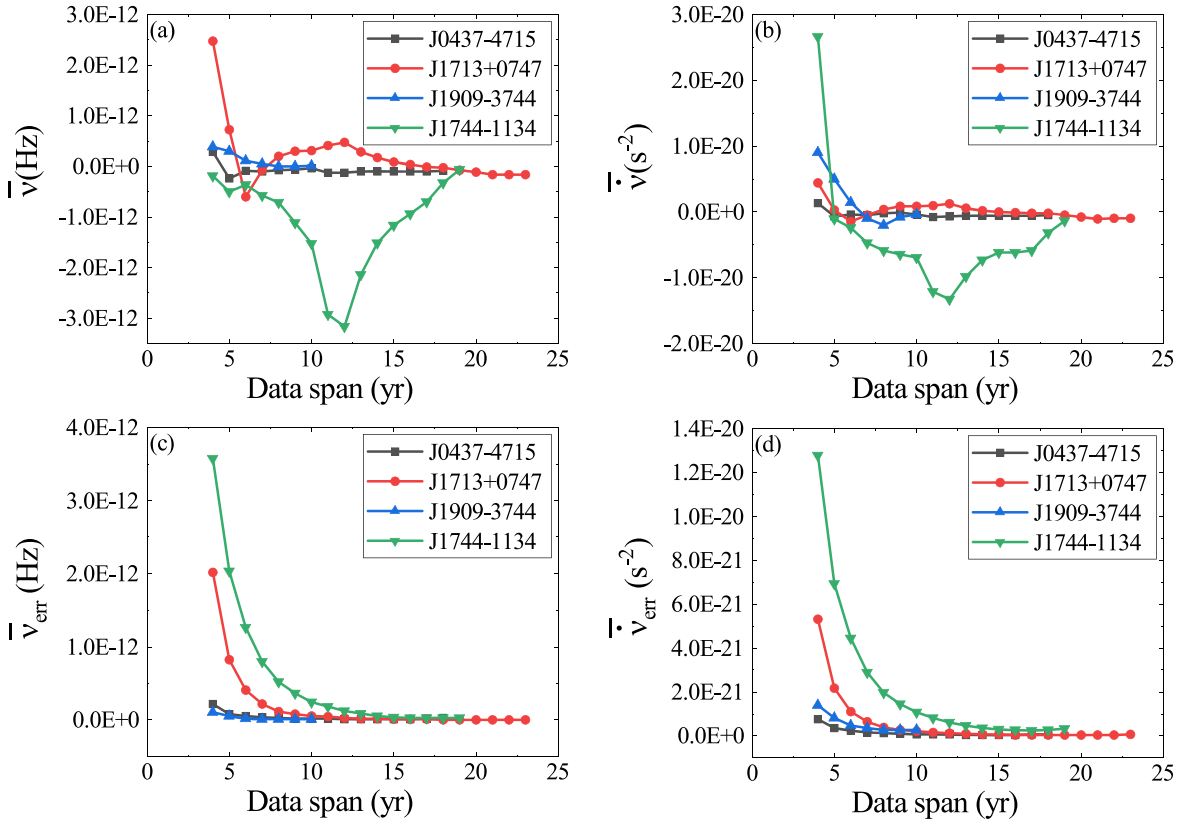

Figure 3. The average of ν and $\dot{\nu}$, determined by different data spans, and their corresponding measurement errors.

observational time span, the data can be divided into 15 overlapping four-year intervals, yielding 15 sets of timing model parameters.

(3) Third, according to the 3σ guidelines, we eliminate the parameters with large errors in 15 sets of pulsar timing model parameters. Then, we compute the average of the remaining parameters, denoted as $\overline{\nu}$ and $\overline{\dot{\nu}}$, to get the average of the pulsar timing model parameters with a four-year data span. Accordingly, we use the error propagation theory to get $\overline{\nu}_{\rm err}$ and $\overline{\dot{\nu}}_{\rm err}$.

(4) Finally, we increase the data span for determining the model parameters with a step of one year and repeat steps (1)–(3) to obtain the average of the pulsar timing model parameters with different data spans.

3.2. Accuracy Analysis

According to the above steps, the corresponding results are shown in Figures 3. Figures 3(a) and (b) show the pulsar timing model parameters for four pulsars, with the initial parameters listed in Table 1 subtracted, across different data spans. Figures 3(c) and (d) show the corresponding measurement errors. To more accurately analyze the variations in pulsar timing model parameters with different data spans, Table 2 shows the differences in pulsar timing model parameters for four pulsars between adjacent data spans. Specifically, when we want to understand the differences in pulsar timing model parameters determined using a five-year data span compared to those determined using a four-year data span, the "Adjacent data span" column in Table 2 would be represented as 5–4, with similar representations for other data-span differences.

3.2.1. PSR J0437-4715

For J0437-4715, as shown in Figures 3(a), (b) and Table 2, the differences in ν determined by two adjacent data spans level off within 10^{-15} Hz when the data span reaches 13 yr or more. Similarly, the differences in the $\dot{\nu}$ level off within $10^{-23}\,{\rm s}^{-2}$. This indicates that the pulsar timing model parameters of J0437-4715 are sufficiently accurate when the data span for determining the pulsar timing model parameters exceeds 13 yr. Among the four pulsars, Figures 3(a) and (b) demonstrate that J0437-4715 exhibits minimal variation in pulsar timing model parameters, which is attributed to its high timing precision and low timing noise.

Typically, spectral analysis of timing residual sequences can estimate the noise level within these residuals. In the field of astronomy, the power spectral density (PSD) of the time series

Table 2
The Differences in Pulsar Timing Model Parameters for Four Pulsars Determined by Adjacent Data Spans

Adjacent Data Span (yr)	$\Delta\overline{\nu}$ (Hz)				$\Delta\overline{\dot{\nu}}(s^{-2})$			
	J0437-4715	J1713+0747	J1744-1134	J1909-3744	J0437-4715	J1713+0747	J1744-1134	J1909-3744
5–4	−5.26969E-13	−1.74677E-12	−3.13484E-13	−9.28019E-14	−2.06307E-21	−4.11584E-21	−2.76623E-20	−4.04872E-21
6–5	1.50550E-13	−1.32738E-12	1.36761E-13	−1.82035E-13	3.67613E-22	−1.76417E-21	−1.31481E-21	−3.53660E-21
7–6	−8.21532E-15	5.24936E-13	−2.21022E-13	−5.73245E-14	−1.11746E-22	9.53173E-22	−2.33007E-21	−2.42491E-21
8–7	2.40546E-14	2.69610E-13	−1.27387E-13	−6.09675E-14	2.66415E-22	8.98243E-22	−1.18600E-21	−1.07213E-21
9–8	1.51745E-14	1.09075E-13	−4.08540E-13	4.92500E-15	1.03047E-22	4.38735E-22	−5.05712E-22	1.25123E-21
10–9	1.54311E-14	1.12162E-14	−4.05101E-13	8.56500E-15	−3.11459E-22	4.81371E-23	−4.76510E-22	3.61476E-22
11–10	–8.10924E-14	9.17202E-14	−1.40271E-12	⋯	−4.01500E-22	3.76538E-23	−5.19191E-21	⋯
12–11	−5.21589E-15	6.87103E-14	−2.36369E-13	⋯	1.47356E-22	2.90662E-22	−1.22527E-21	⋯
13–12	2.69771E-14	−1.90295E-13	1.02106E-12	⋯	1.08123E-22	−6.12861E-22	3.51515E-21	⋯
14–13	−3.46000E-15	−1.10294E-13	6.25118E-13	⋯	−7.51583E-23	−3.64209E-22	2.50475E-21	⋯
15–14	3.72500E-16	−9.25996E-14	3.54339E-13	⋯	2.04163E-23	−2.14408E-22	1.11164E-21	⋯
16–15	3.06083E-15	−4.96057E-14	2.26532E-13	⋯	−2.17942E-24	−8.90458E-23	−1.22974E-23	⋯
17–16	4.31667E-15	−4.95673E-14	2.29479E-13	⋯	3.46042E-23	−1.31945E-22	2.70549E-22	⋯
18–17	1.22300E-14	−1.47898E-14	3.80683E-13	⋯	7.56000E-23	−3.92676E-23	2.73416E-21	⋯
19–18	⋯	−4.48337E-14	2.64560E-13	⋯	⋯	−2.71904E-22	1.80920E-21	⋯
20–19	⋯	−3.23080E-14	⋯	⋯	⋯	−2.26573E-22	⋯	⋯
21–20	⋯	−5.27033E-14	⋯	⋯	⋯	−3.18506E-22	⋯	⋯
22–21	⋯	1.05334E-15	⋯	⋯	⋯	5.21890E-23	⋯	⋯

is usually dominated by red noise, which exhibits a power law behavior in its frequency domain. The power-law model of the red noise is defined as (Coles et al. 2011):

$$P(f) = \frac{A}{(1 + f^2/f_c^2)^{q/2}} \tag{10}$$

where A is the intensity of red noise, f_c is corner frequency, and q is the spectral exponent.

To better analyze the level of red noise for each pulsar, we perform a PSD analysis of the red noise in the post-fit timing residuals, as shown in Figure 4. Figure 4(a) shows the PSD of the red noise of J0437-4715 and the corresponding A, f_c and q. Compared with J1744-1134 and J1713+0747, J0437-4715 has lower red noise intensity, resulting in minimal parameter variation. From Figures 3(c) and (d), we observe that when the data span is within 8 yr, the measurement errors of pulsar timing model parameters for J0437-4715 are significantly smaller than those for J1744-1134 and J1713+0747, which is determined by the measurement accuracy of TOA. As the data span increases, the measurement errors of pulsar timing model parameters gradually decrease and eventually level off, indicating that increasing observations can greatly reduce measurement errors.

3.2.2. PSR J1713+0747

For J1713+0747, as shown in Figures 3(a) and (b), the pulsar timing model parameters exhibit significant variation when the data span for determining these parameters is within 6 yr, which is related to its timing noise. As shown in Figure 4(b), the red noise intensity of J1713+0747 is higher than that of J0437-4715. This higher red noise intensity directly leads to the larger variation in the pulsar timing model parameters for J1713+0747 compared with J0437-4715. From Figures 3(a), (b) and Table 2, it is evident that when the data span exceeds 14 yr, the differences in ν determined by two adjacent data spans level off within 10^{-14} Hz, and the differences in $\dot{\nu}$ level off within $10^{-22}\,s^{-2}$. This indicates that the timing model parameters of J1713+0747 are sufficiently accurate when the data span for determining these parameters exceeds 14 yr. From Figures 3(c) and (d), we can see that J1713 +0747 exhibits larger measurement errors within the 8 yr data span, suggesting that the TOA measurement accuracy for J1713+0747 was relatively poor in the early years. However, with the accumulation of observations and improvements in equipment and techniques, the measurement errors in the pulsar timing model parameters for J1713+0747 approach that of J0437-4715.

3.2.3. PSR J1744-1134

For J1744-1134, Figures 3(a) and (b) show the largest variations in pulsar timing model parameters, which fail to converge even with increasing data spans. This is because J1744-1134 has the worst timing residual accuracy, the least number of TOA, which can be seen from Table 1. As shown in Figure 4(c), the red noise intensity of J1744-1134 is the highest among the four millisecond pulsars. As shown in Figures 3(c) and (d), the measurement errors of pulsar timing model parameters for J1744-1134 are also the largest, indicating that its TOA measurement accuracy is the worst. Although the measurement error of the pulsar timing model parameters tends

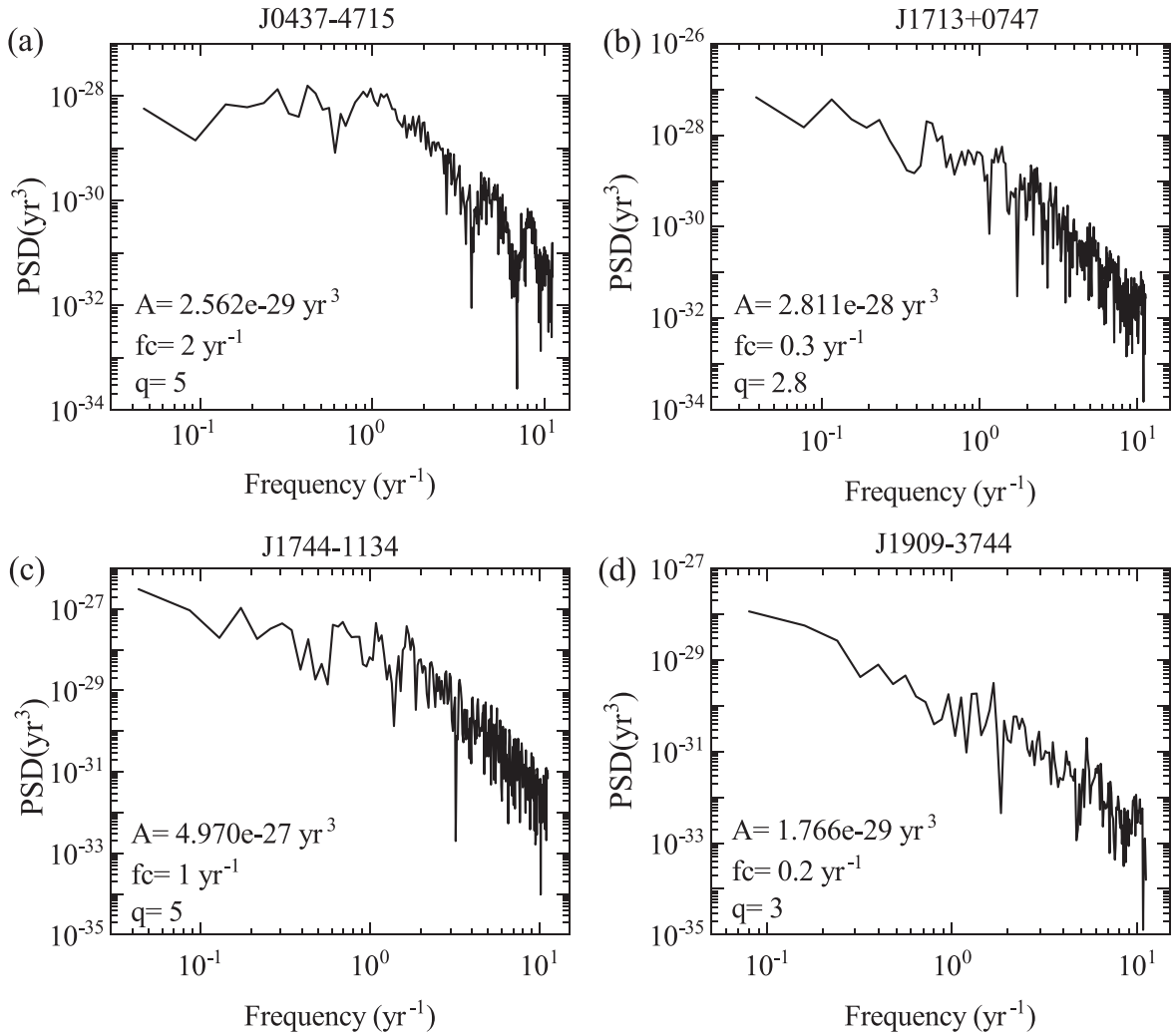

Figure 4. The log–log scale power spectral density of the red noise in the post-fit timing residuals for four pulsars.

to level off when the data span for determining model parameters exceeds 16 yr, it still remains larger than those of the other three pulsars. This indicates that increasing observations alone is insufficient to significantly reduce measurement errors; further improvements in TOA measurement accuracy are necessary.

3.2.4. PSR J1909-3744

For J1909-3744, Table 1 shows that it has the shortest observational time span, which may not meet the minimum convergence span. However, due to the largest number of TOA and the highest timing accuracy, we still discuss its pulsar timing model parameters. As shown in Figures 3(a) and (b), the variations in the pulsar timing model parameters for J1909-3744 are relatively minimal. Table 2 shows that when the data span exceeds 6 yr, the differences in ν determined by two adjacent data spans level off within 10^{-14} Hz, and the difference in $\dot{\nu}$ level off within $10^{-21}\,\mathrm{s}^{-2}$. This demonstrates that the pulsar timing model parameters of J1909-3744 are sufficiently accurate when the data span for determining these parameters exceeds 6 yr. This is due to its highest timing accuracy, the largest number of TOA, and the lowest red noise intensity. As shown in Figure 4(d), the red noise intensity of J1909-3744 is the lowest among the four millisecond pulsars. Figures 3(c) and (d) indicate that the measurement errors of the model parameters for J1909-3744 are relatively small and tend to level off with increasing observations. This demonstrates that J1909-3744 has high TOA measurement accuracy. In summary, J1909-3744 has the highest timing accuracy, the largest number of TOA, the lowest intensity of the red noise, and high TOA measurement accuracy, making it an excellent millisecond pulsar. The primary limitation of J1909-3744 is its relatively short observational time span. Nevertheless, as more

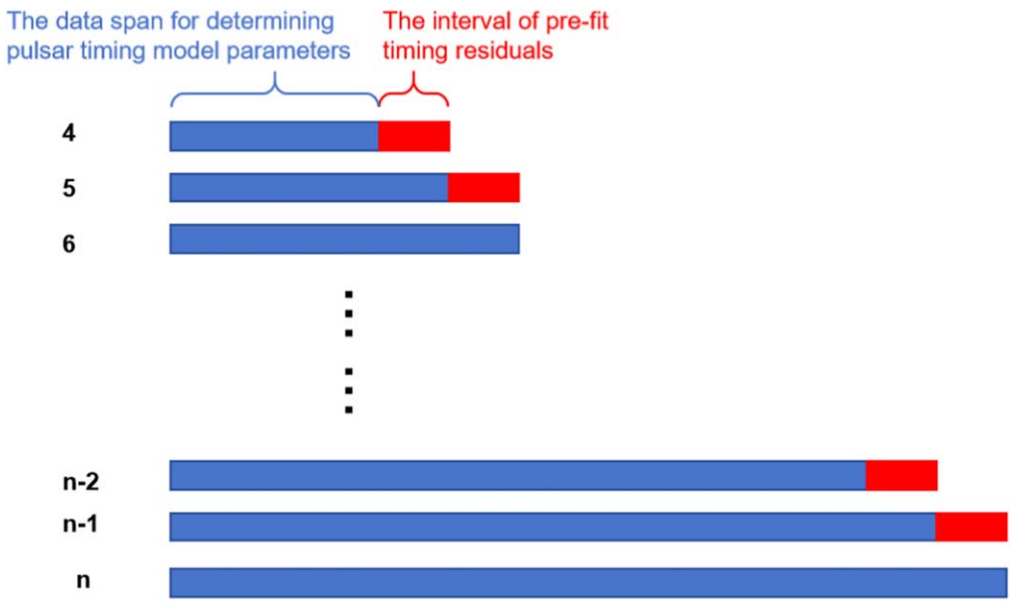

Figure 5. Schematic diagram of data spans for determining pulsar timing model parameters and pre-fit timing residuals intervals. The blue part represents the data spans for determining pulsar timing model parameters, and the red part represents the intervals of pre-fit timing residuals predicted by the model parameters in the previous blue part. k_p is the slope of the pre-fit timing residuals in the red part. k_r can be computed from ν for two adjacent data spans in the blue part.

observations are accumulated, the precision of its timing model parameters is expected to improve, establishing it as a prime candidate for future pulsar-based timekeeping studies.

4. Accuracy Analysis of TT(PT) on a One-year Timescale

Sufficient accuracy is a prerequisite for TT(PT) to serve as a timescale. Therefore, after determining the accurate pulsar timing model parameters, we also discuss the accuracy of the TT(PT) on a one-year timescale predicted by the model parameters.

4.1. Accuracy Calculations

Once the model parameters are determined, the pre-fit timing residuals can be predicted by Equation (8). The absolute value of the slope of the pre-fit timing residuals, denoted as k_p, reflects the frequency deviation of the TT(PT) relative to TT(BIPM15). The causes of this frequency deviation include the rotational characteristics of pulsars, inaccuracy in the timing model parameters, timing noise, fitting errors, and so on. The smaller the frequency deviation, the higher the accuracy of the TT(PT). Additionally, the relative frequency deviation (k_r), derived from ν determined over two adjacent data spans, also reflects the frequency deviation of TT(PT) relative to TT(BIPM15). The data spans for determining pulsar timing model parameters are shown in the blue part of Figure 5. The k_r between two adjacent data spans for determining pulsar timing model parameters can be expressed as follows:

$$k_{rnm} = \left| \frac{\nu_{n,m} - \nu_{n-1,m}}{\nu_{n-1,m}} \right| (n \geqslant 4) \tag{11}$$

where $\nu_{n,m}$ is the rotational frequency (ν) in the mth set of timing model parameters, which is determined over a data span of n years. We use the last-year interval (red part in Figure 5) to examine the prediction of the pulsar clock according to the pre-fit timing residuals in the same interval. The method for determining pulsar timing model parameters is the same as in step 3.1.1, with the prediction interval being the adjacent one-year interval to the data span for determining model parameters, as shown in the red part of Figure 5. k_{pnm} is the slope of the one-year pre-fit timing residuals predicted by the mth set of timing model parameters, which is determined over a data span of n years. k_r depends on two sets of ν determined by two adjacent data spans and reflects the optimal level of TT(PT) in an ideal situation. In contrast, k_p reflects the accuracy of TT(PT) in the actual situation.

4.2. Accuracy Analysis

To evaluate the accuracy of k_p and k_r, we selected another time reference—TT(TAI). We calculate the relative frequency deviation of TT(TAI) relative to TT(BIPM15) over the same interval as the pre-fit timing residuals, denoted as $k_{\rm tai}$. Then we conduct a detailed comparative analysis of k_p, k_r, and $k_{\rm tai}$ in different intervals.

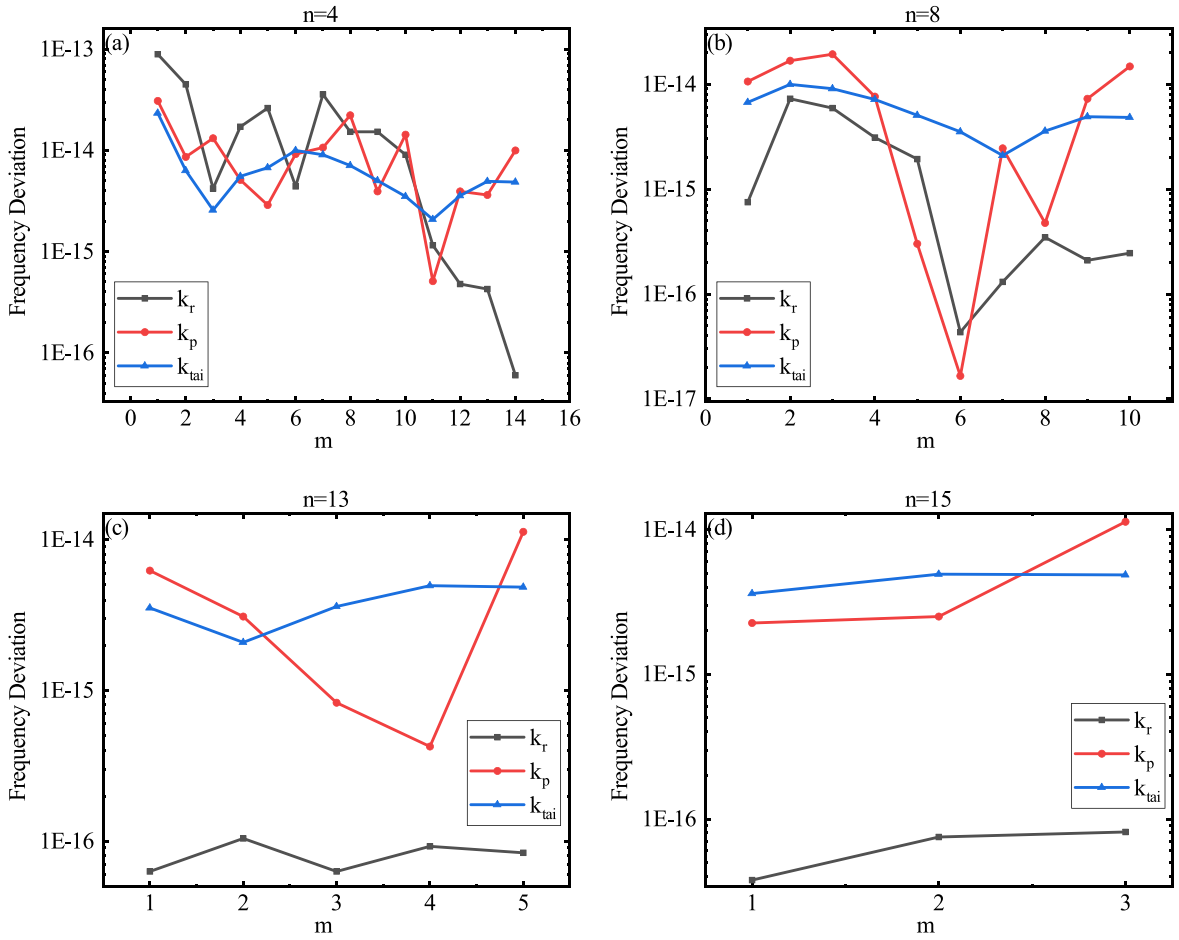

Figure 6. The comparison chart of k_r, k_p and $k_{\rm tai}$ for J0437-4715, determined by data spans of 4, 8, 13, and 15 yr, respectively. The horizontal axis represents the ordinal sequence of the timing model parameter sets, and n denotes the data span for determining pulsar timing model parameters. The black line represents k_r, the red line represents k_p, and the blue line represents $k_{\rm tai}$.

4.2.1. PSR J0437-4715

For the 18.6 yr observational time span of PSR J0437-4715, we divided the time span into 15 data spans for determining pulsar timing model parameters and 14 pre-fit timing residuals prediction intervals, resulting in 14 comparative cases. We selected representative intervals of 4, 8, 13, and 15 yr for demonstration, as shown in Figure 6. As indicated in Section 3, the timing model parameters of PSR J0437-4715 vary significantly within 6 yr and tend to level off after 13 yr. As shown in Figure 6, when the data span for determining pulsar timing model parameters is less than 6 yr, k_r and k_p are relatively close. However, as the data span increases, the difference between them gradually becomes significant, particularly when the data span exceeds 13 yr. This is because k_p is always affected by timing noise and other uncertainty factors, regardless of the model parameters. While k_r is minimally affected by the uncertainties factors once the model parameters level off, approaching an ideal situation. Therefore, when the data span for determining pulsar timing model parameters is less than 6 yr, k_p and k_r are both influenced by timing noise and other uncertainty factors, resulting in minimal differences. After the pulsar timing model parameters are accurately determined, the k_p is still influenced by timing noise and other uncertainty factors, whereas the k_r is nearly ideal, resulting in significant differences.

It is worth noting that with an 8 yr data span for determining pulsar timing model parameters, k_r and k_p have similar trends in the first eight data spans, but differ significantly afterward. This is attributed to the continuous improvement in TOA measurement accuracy due to advancements in observational technology and telescope equipment, where the pulsar timing model parameters based on later observations are more accurate than those based on early observations. As the data span for determining pulsar timing model parameters increases, k_p decreases, indicating improved TT(PT) accuracy. To more intuitively analyze the variation of k_p, k_r, and $k_{\rm tai}$ over different

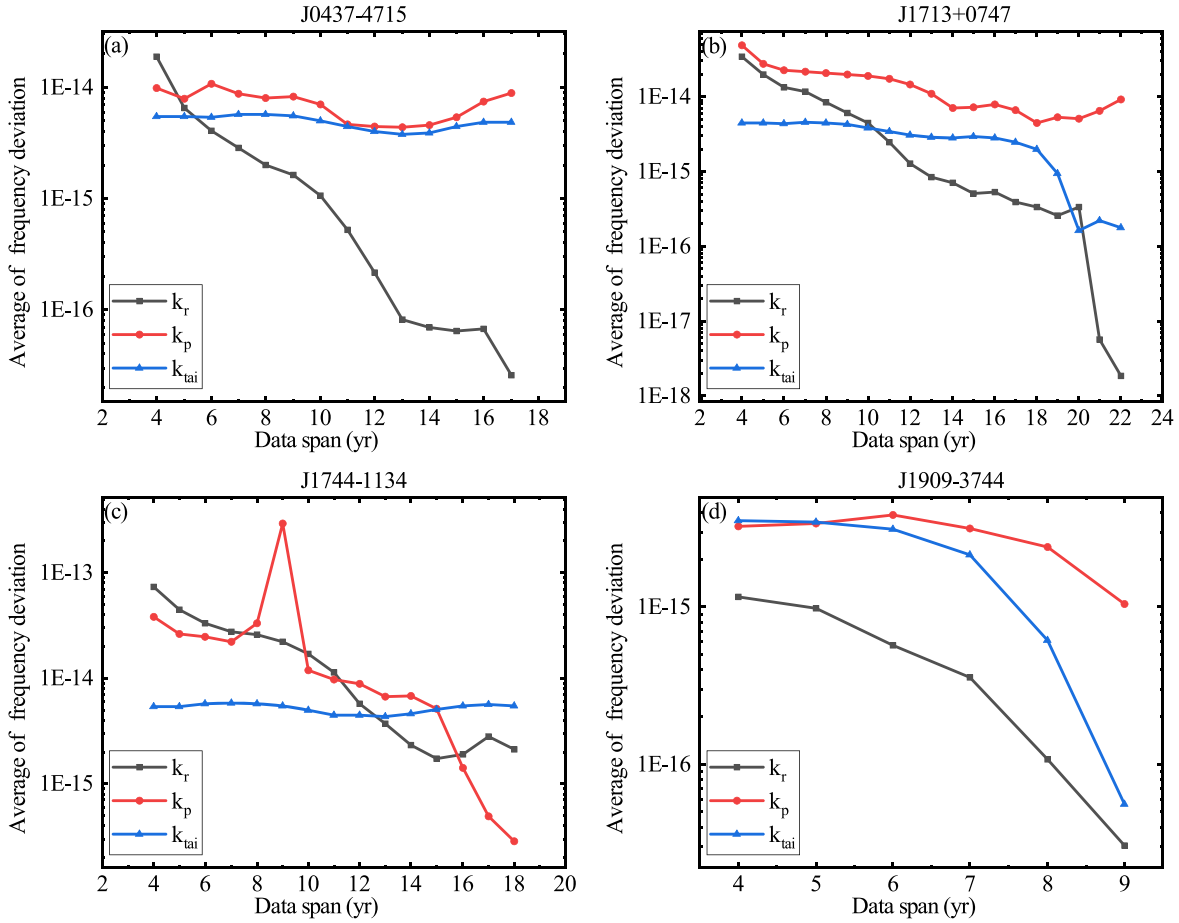

Figure 7. The comparison chart of the average of k_p, k_r and k_{tai} for four pulsars determined by different data spans respectively. The horizontal axis represents the data span for determining pulsar timing model parameters. The black line represents k_r, the red line represents k_p, and the blue line represents k_{tai}.

data spans for determining pulsar timing model parameters, we remove outliers from k_p, k_r, and k_{tai} over different data spans according to the 3σ guidelines. Subsequently, we calculate the average of the remaining data, as shown in Figure 7(a) and Table 3. The results indicate that when the data span for determining pulsar timing model parameters is less than 5 yr, the accuracy of k_r is inferior to k_{tai}. When the data span exceeds 5 yr, the accuracy of k_r rapidly improves, stabilizing after 13 yr and surpassing k_{tai}. This demonstrates the critical importance of long-term observations for determining accurate pulsar timing model parameters. For k_p, although its accuracy is always inferior to k_{tai}, it still improves with increasing data spans. When the data span exceeds 13 yr, the accuracy of the one-year pre-fit timing residual prediction by these model parameters is slightly lower than TT(TAI). Considering the long-term stability of pulsars, we speculate that the accuracy of pre-fit timing residuals on timescale longer than one year could be

Table 3
The Averages of k_p, k_r and k_{tai} for J0437-4715 Determined by Adjacent Data Spans

Adjacent Data Span (yr)	k_r	k_p	k_{tai}
5–4	1.87464E-14	9.91014E-15	5.47936E-15
6–5	6.51267E-15	7.88485E-15	5.47936E-15
7–6	4.06189E-15	1.07356E-14	5.40858E-15
8–7	2.84733E-15	8.69419E-15	5.66726E-15
9–8	1.98797E-15	7.96156E-15	5.68245E-15
10–9	1.62346E-15	8.22688E-15	5.56878E-15
11–10	1.05843E-15	6.98488E-15	5.02241E-15
12–11	5.24635E-16	4.64941E-15	4.43838E-15
13–12	2.15808E-16	4.46329E-15	3.99487E-15
14–13	8.14449E-17	4.35902E-15	3.78928E-15
15–14	6.97947E-17	4.56805E-15	3.85923E-15
16–15	6.46178E-17	5.34543E-15	4.45387E-15
17–16	6.76213E-17	7.44016E-15	4.88195E-15
18–17	2.58510E-17	8.92026E-15	4.83685E-15

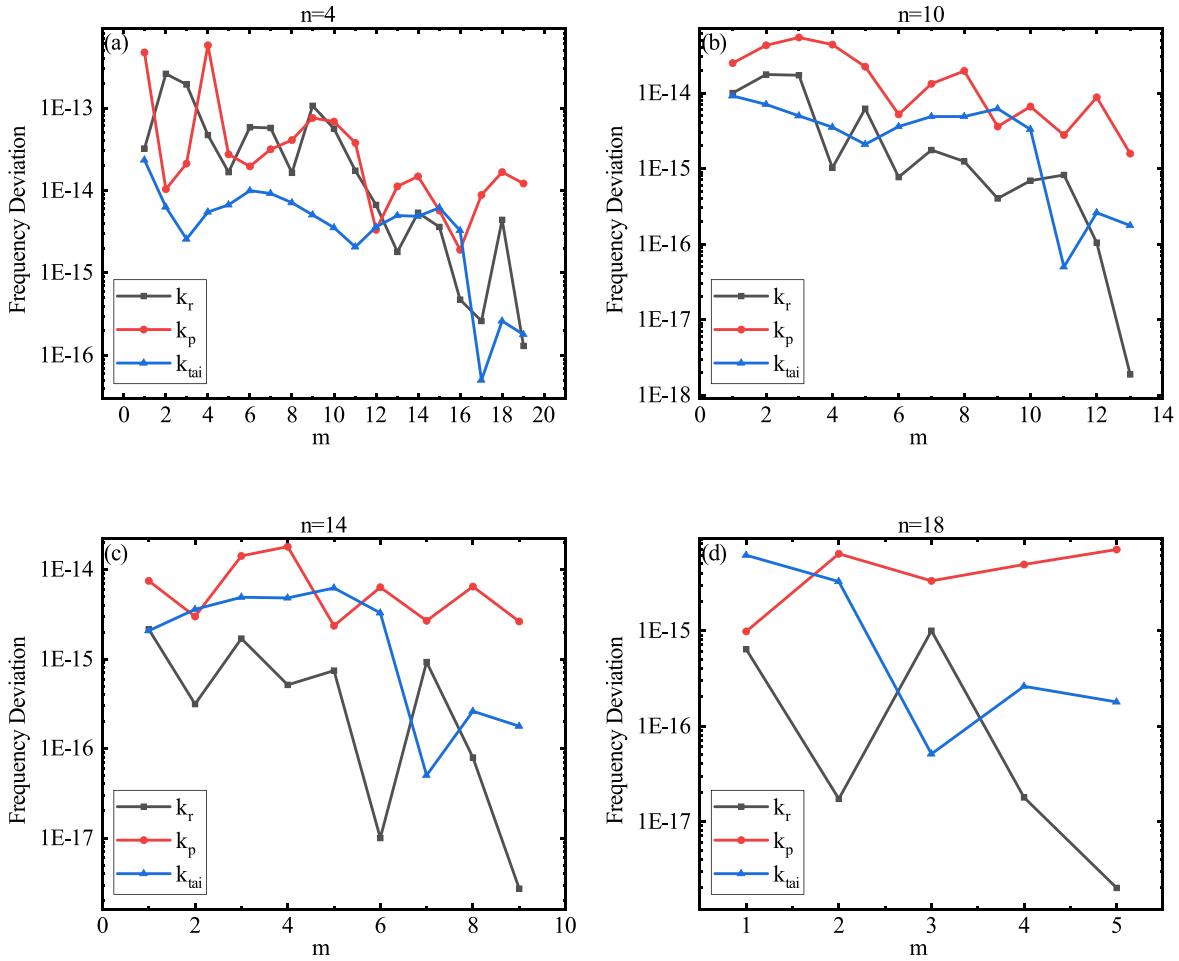

Figure 8. The comparison chart of k_r, k_p and $k_{\rm tai}$ for J1713+0747, determined by data spans of 4, 10, 14, and 18 yr, respectively. The horizontal axis represents the ordinal sequence of the timing model parameter sets, and n denotes the data span for determining pulsar timing model parameters. The black line represents k_r, the red line represents k_p, and the blue line represents $k_{\rm tai}$.

comparable to TT(TAI). k_r represents the optimal achievable level of TT(PT) under ideal conditions. With the continuous accumulation of observations and advancements in observation technology, the accuracy of TT(PT) is expected to increasingly approach this ideal state.

4.2.2. PSR J1713+0747

For the 22.5 yr observational time span of PSR J1713+0747, we divided the time span into 20 data spans for determining pulsar timing model parameters and 19 pre-fit timing residuals prediction intervals, resulting in 19 comparative cases. We selected representative intervals of 4, 10, 14, and 18 yr for demonstration, as shown in Figure 8. From Section 3, it is apparent that the pulsar timing model parameters for PSR 1713 +0747 show significant variations within 6 yr and tend to level off after 14 yr. As can be seen from Figure 8, the trends in the variations of k_p and k_r are similar to those observed for PSR J0437-4715. That is, as the data span for determining model parameters increases, the difference between k_r and k_p increases, and the accuracy of the model parameters improves. Figures 8(a)–(d) shows the detailed process of gradual increase in the difference between k_p and k_r. Similarly, the pulsar timing model parameters based on late observations are more accurate than those based on early observations, driven by improvements in measurement accuracy. Additionally, we remove outliers from k_p, k_r, and $k_{\rm tai}$ over different data spans according to the 3σ guidelines, and calculate the average of the remaining data, as shown in Figure 7(b) and Table 4. The results indicate that when the data span for determining pulsar timing model parameters is less than 10 yr, the accuracy of k_r is inferior to that of $k_{\rm tai}$. However, when the data span exceeds 10 yr, the accuracy of the k_r gradually surpasses that of $k_{\rm tai}$. This further substantiates the importance of long-term observations for determining accurate pulsar timing model parameters. The accuracy of k_p slightly improves as the data span increases, yet

Table 4
The Averages of k_p, k_r and k_{tai} for J1713+0747 Determined by Adjacent Data Spans

Adjacent Data Span (yr)	k_r	k_p	k_{tai}
5–4	3.42027E-14	4.85160E-14	4.50938E-15
6–5	1.99256E-14	2.75635E-14	4.50938E-15
7–6	1.32732E-14	2.26183E-14	4.40236E-15
8–7	1.16674E-14	2.17047E-14	4.51731E-15
9–8	8.48964E-15	2.06040E-14	4.45077E-15
10–9	6.04061E-15	1.97097E-14	4.28972E-15
11–10	4.45130E-15	1.92155E-14	3.85511E-15
12–11	2.47576E-15	1.73001E-14	3.41715E-15
13–12	1.29031E-15	1.46178E-14	3.08239E-15
14–13	8.49913E-16	1.09570E-14	2.88835E-15
15–14	7.12027E-16	7.01646E-15	2.81934E-15
16–15	5.05343E-16	7.16985E-15	2.91234E-15
17–16	5.31540E-16	7.94903E-15	2.81443E-15
18–17	3.93725E-16	6.56037E-15	2.46233E-15
19–18	3.31088E-16	4.50078E-15	1.98742E-15
20–19	2.54305E-16	5.35706E-15	9.39673E-16
21–20	3.32813E-16	5.08534E-15	1.63248E-16
22–21	5.64412E-18	6.53761E-15	2.19696E-16

consistently remains inferior to k_{tai}. Compared with PSR J0437-4715, PSR J1713+0747 demonstrates a slower improvement in the accuracy of k_r and inferior accuracy in k_p. This is because the red noise intensity of PSR J1713+0747 is higher than that of PSR J0437-4715 and the measurement accuracy of TOA is worse than that of PSR J0437-4715. Similarly to PSR J0437-4715, after the pulsar timing model parameters level off, the accuracy of k_r surpasses that of k_{tai}, while the accuracy of k_p is inferior to k_{tai}. This implies that, with continuous improvements in observational technology, there is potential for further improvement in the accuracy of TT(PT).

4.2.3. PSR J1744-1134

For the 19.9 yr observational time span of PSR J1744-1134, we divided the time span into 16 data spans for determining pulsar timing model parameters and 15 pre-fit timing residuals prediction intervals, resulting in 15 comparative cases. We selected representative intervals of 4, 8, 13, and 17 yr for demonstration, as shown in Figure 9. As illustrated in Figure 9, a significant difference between k_r and k_p is observed only when the data span reaches 17 yr. This demonstrates that the timing model parameters of J1744-1134 do not level off when the data span is less than 17 yr, which is related to its worst timing accuracy, highest red noise intensity, and sparsest observations. Across different data spans, we still remove outliers from k_p, k_r, and k_{tai} according to the 3σ guidelines and calculate the average of the remaining data, as shown in Figure 7(c) and Table 5. As can be seen from Figure 7(c), as the data span increases, k_r decreases and its accuracy increases. When the data span exceeds 13 yr, the accuracy of k_r surpasses that of k_{tai}. However, compared with the other three pulsars, the accuracy of k_r for PSR J1744-1134 remains the worst. For k_p, its accuracy also improves with increasing data spans. Within the data span of 15 yr, the accuracy of k_p is inferior to that of k_{tai}, but it surpasses k_{tai} when the data span exceeds 15 yr. Furthermore, the accuracy of k_p surpasses that of k_r when the data span for determining pulsar timing model parameters exceeds 15 yr, which is anomalous. The anomalies may be attributed to randomness and fitting errors during the fitting process, which are caused by the worst measurement precision and highest red noise intensity of PSR J1744-1134.

4.2.4. PSR J1909-3744

For the 10.8 yr observational time span of PSR J1909-3744, we divided the time span into seven data spans for determining pulsar timing model parameters and six pre-fit timing residuals prediction intervals, resulting in six comparative cases. We selected representative intervals of 4, 5, 6, and 8 yr for demonstration, as shown in Figure 10. As indicated in Section 3, the overall variation in the pulsar timing model parameters for PSR J1909-3744 is minimal and tends to level off after 6 yr. As shown in Figure 10, the difference between k_r and k_p for PSR J1909-3744 becomes distinctly apparent under the data span of 5 yr. This can be attributed to its high timing accuracy and low noise intensity, which allows us to obtain accurate pulsar timing model parameters with a short data span. Moreover, pulsar timing model parameters determined by newer observations consistently exhibit higher accuracy compared with those determined by older observations. Across different data spans, we also remove outliers from k_p, k_r, and k_{tai} according to the 3σ guidelines, and calculate the average of the remaining data, as shown in Figure 7(d) and Table 6. As can be seen from Figure 7(d) and Table 6, the k_r of PSR J1909-3744 decreases with increasing data span, and its accuracy improves. And the accuracy of k_r always surpasses that of k_{tai}. The accuracy of k_p slightly improves as the data span increases, but remains slightly inferior to k_{tai}. Compared with the J0437-4715 and J1713+0747, the accuracy of the k_p for PSR J1909-3744 is greatly improved, which is attributable to the excellent properties of PSR J1909-3744, including high timing accuracy and low timing noise. Despite the shorter observational time span of PSR J1909-3744, its high accuracy still makes it a primary object of study in the pulsar timescale. As the observations continue to accumulate, the accuracy of TT(PT) is expected to improve further.

5. Conclusions

We studied the effect of different data spans for determining pulsar timing model parameters on the accuracy of these parameters and discussed the accuracy of TT(PT) established by

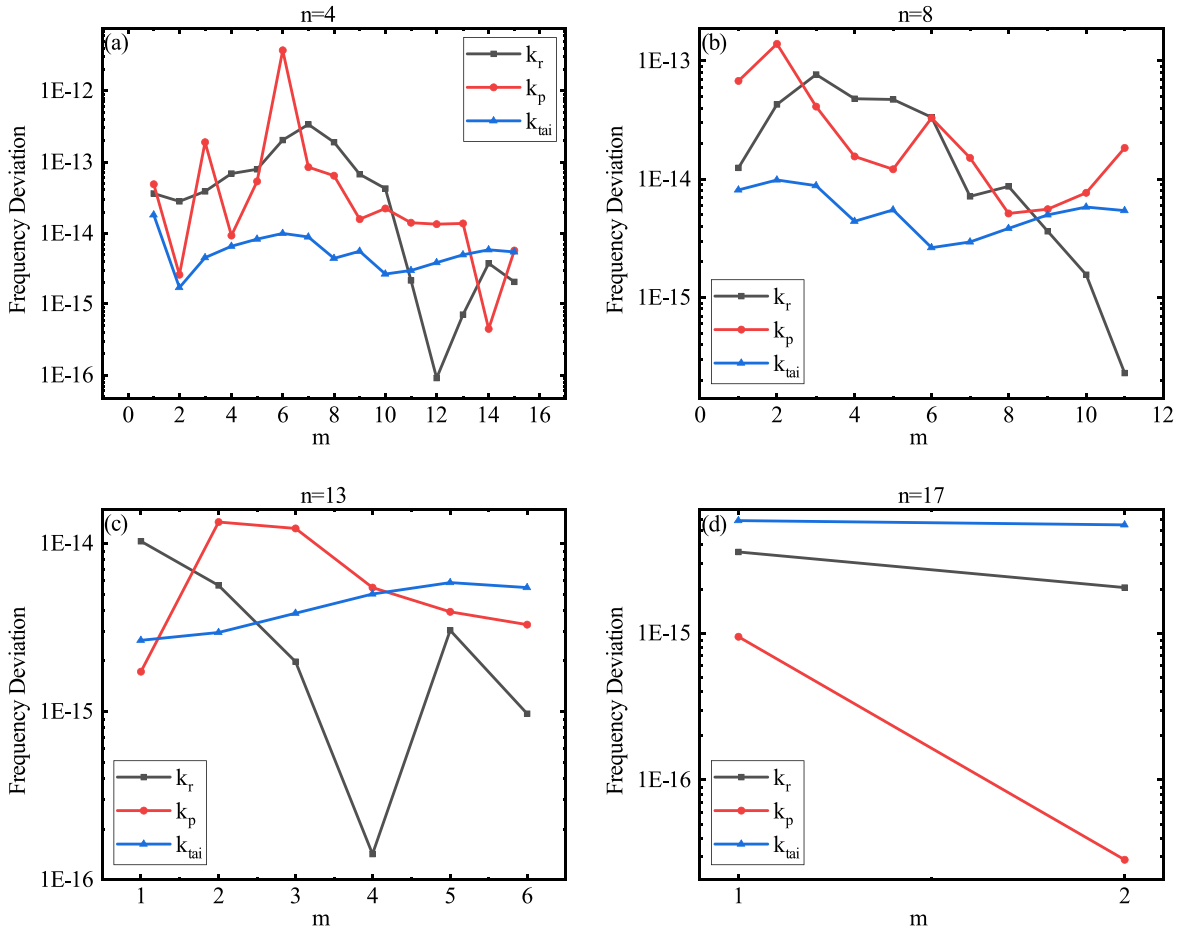

Figure 9. The comparison chart of k_r, k_p and $k_{\rm tai}$ for J1744-1134, determined by data spans of 4, 8, 13, and 17 yr, respectively. The horizontal axis represents the ordinal sequence of the timing model parameter sets, and n denotes the data span for determining pulsar timing model parameters. The black line represents k_r, the red line represents k_p, and the blue line represents $k_{\rm tai}$.

Table 5
The Averages of k_p, k_r and $k_{\rm tai}$ for J1744-1134 Determined by Adjacent Data Spans

Adjacent Data Span (yr)	k_r	k_p	$k_{\rm tai}$
5–4	7.31870E-14	3.83281E-14	5.39573E-15
6–5	4.43152E-14	2.63391E-14	5.39573E-15
7–6	3.31355E-14	2.47744E-14	5.67959E-15
8–7	2.76954E-14	2.21231E-14	5.77671E-15
9–8	2.57155E-14	3.29338E-14	5.70580E-15
10–9	2.19763E-14	2.94175E-13	5.46051E-15
11–10	1.70317E-14	1.17980E-14	4.96632E-15
12–11	1.13421E-14	9.73292E-15	4.47295E-15
13–12	5.70365E-15	8.81513E-15	4.47641E-15
14–13	3.67866E-15	6.69310E-15	4.29967E-15
15–14	2.30540E-15	6.80680E-15	4.62849E-15
16–15	1.72577E-15	5.15015E-15	5.04721E-15
17–16	1.89756E-15	1.40373E-15	5.44331E-15
18–17	2.81608E-15	4.88464E-16	5.66577E-15
19–18	2.10381E-15	2.85306E-16	5.45919E-15

these model parameters. From IPTA DR2, we selected four pulsars with high timing precision, J0437-4715, J1713+0747, J1744-1134, and J1909-3744, as our study objects. We determined the pulsar timing model parameters with an initial four-year data span. Based on the initial data span, we divided the total time span into different intervals. At this data span, we obtained multiple sets of pulsar timing model parameters with different data intervals. We calculated the averages of ν and $\dot{\nu}$ from these sets of pulsar timing model parameters. Then we increased the data span in steps of one year, similarly computing the averages of ν and $\dot{\nu}$. The timing model parameters are sufficiently accurate when the averages of ν and $\dot{\nu}$ tend to level off over different data spans. The results indicated that when the data span exceeds 13 yr, the amplitude of fluctuations in ν for PSR J0437-4715 remains within 10^{-15} Hz, and the amplitude of fluctuations in $\dot{\nu}$ remains within 10^{-23} s^{-2}. For PSR J1713+0747, when the data span exceeds 14 yr, the amplitude of fluctuations in ν and $\dot{\nu}$ remain within 10^{-14} Hz and 10^{-22} s^{-2}, respectively. For

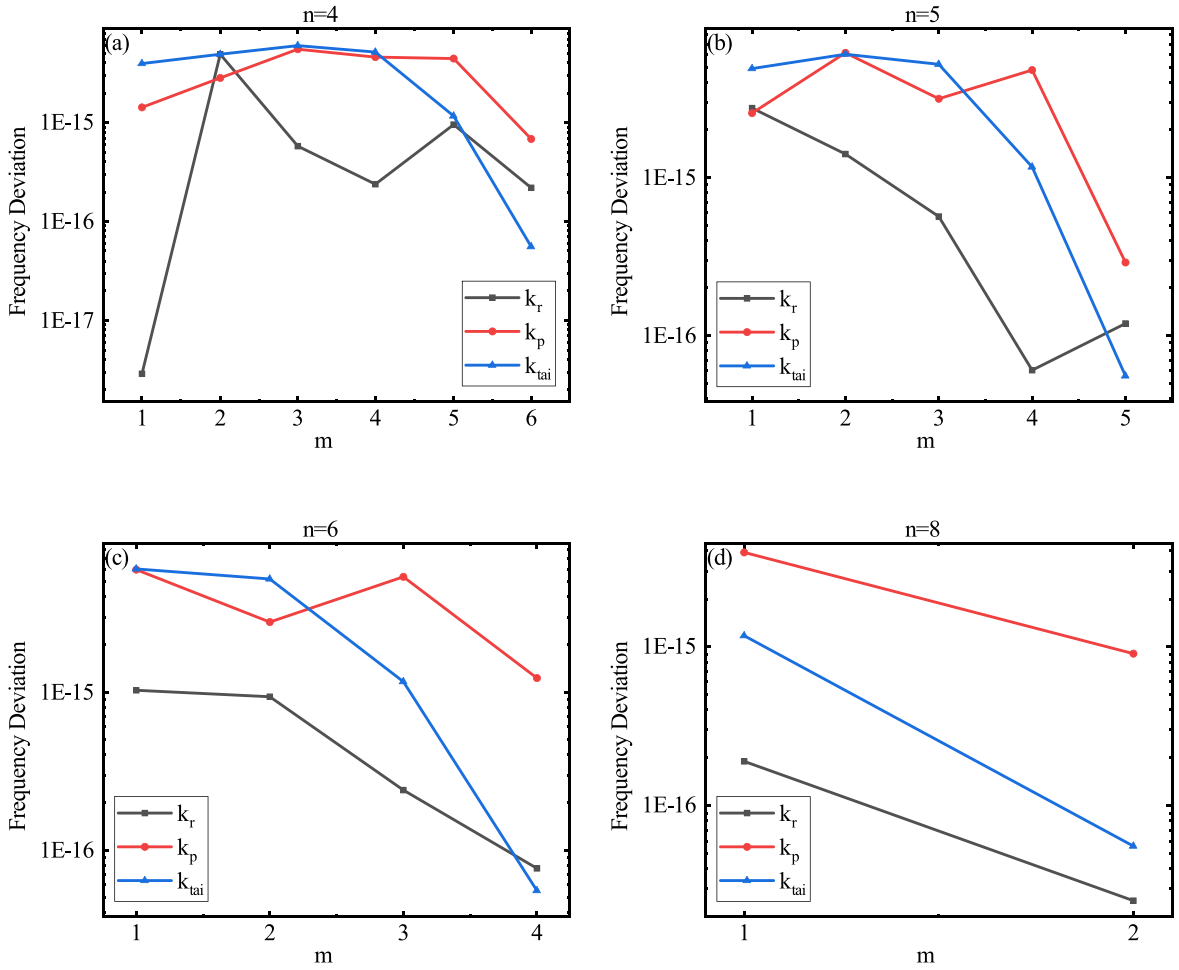

Figure 10. The comparison chart of k_r, k_p and k_{tai} for J1909-3744, determined by data spans of 4, 5, 6, and 8 yr, respectively. The horizontal axis represents the ordinal sequence of the timing model parameter sets, and n denotes the data span for determining pulsar timing model parameters. The black line represents k_r, the red line represents k_p, and the blue line represents k_{tai}.

PSR J1909-3744, when the data span exceeds 6 yr, the amplitude of fluctuations in ν remains within 10^{-14} Hz, and the amplitude of fluctuations in $\dot{\nu}$ remains within 10^{-21} s^{-2}. For J1744-1134, the ν and $\dot{\nu}$ do not tend to level off across different data spans, due to its worse properties.

After exploring the effect of data span on pulsar timing model parameters, we discussed the one-year accuracy of TT(PT) established by these model parameters. Following the same steps as mentioned above, using an initial four-year data span, we obtained multiple sets of pulsar timing model parameters with different data intervals. Then we calculated the accuracy (k_p) of TT(PT) predicted by the multiple set of model parameters in the actual case and the accuracy (k_r) of TT(PT) established in the ideal case. Still increasing the data span in steps of one year, k_p and k_r were calculated for different timing model parameters. To assess the one-year accuracy of k_p and k_r, corresponding results given by TT(TAI) were also studied for comparison.

Table 6
The Averages of k_p, k_r and k_{tai} for J1909-3744 Determined by Adjacent Data Spans

Adjacent Data Span (yr)	k_r	k_p	k_{tai}
5–4	1.15545E-15	3.26845E-15	3.54741E-15
6–5	9.79171E-16	3.38201E-15	3.46742E-15
7–6	5.71032E-16	3.84508E-15	3.11046E-15
8–7	3.54989E-16	3.14865E-15	2.13945E-15
9–8	1.07363E-16	2.41430E-15	6.13613E-16
10–9	3.03552E-17	1.04065E-15	5.54282E-17

The results showed that the one-year accuracy of the TT(PT) established by timing model parameters is related to the properties of the pulsars, including timing precision, noise intensity, and the number of TOA. Among the four pulsars, J1909-3744 had the best properties, resulting in the highest

accuracy of TT(PT) established by its timing model parameters. Conversely, J1744-1134 had the worst properties, resulting in the lowest accuracy of TT(PT) established by its timing model parameters, and exhibited an anomalous phenomenon where k_p surpassed k_r after a data span of more than 16 yr. This indicates that J1744-1134 is not a good object for single TT(PT) studies. For J0437-4715, J1713+0747, and J1909-3744, once the timing model parameters level off, k_r consistently surpassed $k_{\rm tai}$, while k_p was consistently inferior to $k_{\rm tai}$. This suggests that for these three pulsars, the one-year accuracy of TT(PT) under the ideal case is superior to TT(TAI). Although currently, the one-year accuracy of TT(PT) in the actual case is lower than TT(TAI). However, with the continuous accumulation of observations and improvements in observation precision, the one-year accuracy of k_r is expected to be comparable to that of $k_{\rm tai}$. This provides a theoretical basis for using TT(PT) as a time standard.

Acknowledgments

This work was supported by the Strategic Priority Research Program of Chinese Academy of Sciences (grant No. XDA0350502), the National SKA Program of China (No. 2020SKA0120103) and the National Natural Science Foundation of China (No. U1831130).

References

Arzoumanian, Z., Baker, P. T., Blumer, H., et al. 2020, ApJL, 905, L34
Backer, D. C., Kulkarni, S. R., Heiles, C. H., Davis, M. M., & Goss, W. M. 1982, Natur, 300, 615
Coles, W., Hobbs, G., Champion, D. J., Manchester, R. N., & Verbiest, J. P. W. 2011, MNRAS, 418, 561
Davis, M. M., Taylor, J. H., Weisberg, J. M., & Backer, D. C. 1985, Natur, 315, 547
Desvignes, G., Caballero, R. N., Lentati, L., et al. 2016, MNRAS, 458, 3341
Edwards, R. T., Hobbs, G. B., & Manchester, R. N. 2006, MNRAS, 372, 1549
Guinot, B., & Petit, G. 1991, A&A, 248, 292
Hewish, A., Bell, S. J., Pilkingt, J. D., Scott, P. F., & Collins, R. A. 1968, Natur, 217, 709
Hobbs, G. B., Edwards, R. T., & Manchester, R. N. 2006, MNRAS, 369, 655
Hobbs, G., Coles, W., Manchester, R. N., et al. 2012, MNRAS, 427, 2780
Hobbs, G., Guo, L., Caballero, R. N., et al. 2020, MNRAS, 491, 5951
Johnston, S., Karastergiou, A., Keith, M. J., et al. 2020, MNRAS, 493, 3608
Lee, K. J. 2016, in ASP Conf. Ser. 502, Frontiers in Radio Astronomy and FAST Early Sciences Symp. 2015, ed. L. Qian (San Francisco, CA: ASP), 19
Lyne, A., & Graham-Smith, F. 2012, Pulsar Astronmy (Cambridge: Cambridge Univ. Press), 1
Panfilo, G., & Arias, F. 2009, Studies and possible improvements on EAL algorithm, in Joint Meeting of the 23rd European Frequency and Time Forum/IEEE Int. Frequency Control Symp. (Besancon, France: IEEE), 110
Perera, B. B. P., DeCesar, M. E., Demorest, P. B., et al. 2019, MNRAS, 490, 4666
Petit, G. 2004, A New Realization of Terrestrial Time (France: BIPM)
Piriz, R., Garbin, E., Roldan, P., et al. 2019, Annual Precise Time and Time Interval Systems and Applications Meeting (Washington: Inst. Navigation), 191
Reardon, D. J., Shannon, R. M., Cameron, A. D., et al. 2021, MNRAS, 507, 2137
Reichley, P., Downs, G., & Morris, G. 1971, JPLQT, 1, 80
Rodin, A. E. 2008, MNRAS, 387, 1583
Tarafdar, P., Nobleson, K., Rana, P., et al. 2022, PASA, 39, e053
Taylor, J. H. 1991, Proc. IEEE, 79, 1054
Tong, M. L., Yang, T. G., Zhao, C. S., & Gao, Y. P. 2017, SSPMA, 47, 099503
Verbiest, J. P. W., Lentati, L., Hobbs, G., et al. 2016, MNRAS, 458, 1267
Zhang, Z., Tong, M., & Yang, T. 2024, ApJ, 962, 2